Different Rho GTPase–dependent signaling pathways initiate sequential steps in the consolidation of long-term potentiation

Christopher S. Rex,[1] Lulu Y. Chen,[2] Anupam Sharma,[2] Jihua Liu,[2] Alex H. Babayan,[2] Christine M. Gall,[2,3] and Gary Lynch[1,2]

[1]Department of Psychiatry and Human Behavior, [2]Department of Anatomy and Neurobiology, and [3]Department of Neurobiology and Behavior, University of California, Irvine, Irvine, CA 92697

The releasable factor adenosine blocks the formation of long-term potentiation (LTP). These experiments used this observation to uncover the synaptic processes that stabilize the potentiation effect. Brief adenosine infusion blocked stimulation-induced actin polymerization within dendritic spines along with LTP itself in control rat hippocampal slices but not in those pretreated with the actin filament stabilizer jasplakinolide. Adenosine also blocked activity-driven phosphorylation of synaptic cofilin but not of synaptic p21-activated kinase (PAK). A search for the upstream origins of these effects showed that adenosine suppressed RhoA activity but only modestly affected Rac and Cdc42. A RhoA kinase (ROCK) inhibitor reproduced adenosine's effects on cofilin phosphorylation, spine actin polymerization, and LTP, whereas a Rac inhibitor did not. However, inhibitors of Rac or PAK did prolong LTP's vulnerability to reversal by latrunculin, a toxin which blocks actin filament assembly. Thus, LTP induction initiates two synaptic signaling cascades: one (RhoA-ROCK-cofilin) leads to actin polymerization, whereas the other (Rac-PAK) stabilizes the newly formed filaments.

Introduction

Extreme persistence is a defining property of long-term potentiation (LTP; Abraham, 2003) and perhaps the most striking of its many correspondences with memory. However, although the ultimate form of LTP is remarkably stable, its initial expression is easily disrupted by any of several manipulations. The time-dependent process whereby LTP is made resistant to disturbance (consolidation) is known to have at least two phases: an initial stage lasting 10–30 min followed by a slower, protein synthesis–dependent step (Morris et al., 2003; Lynch et al., 2007).

Certain characteristics of LTP (rapid appearance, persistence, and synapse specificity) led to the proposal that rapid consolidation involves modifications to the subsynaptic cytoskeleton (Matus et al., 1982; Lynch and Baudry, 1984). In accord with this, induction of LTP in adult hippocampus causes the rapid emergence of F-actin in individual dendritic spines (Fukazawa et al., 2003; Lin et al., 2005) that, like LTP itself, is transiently vulnerable to disruption (Kramar et al., 2006). Accordingly, actin filament assembly blockers destabilize LTP without affecting its initial expression (Krucker et al., 2000). These findings suggest that cytoskeletal events are central to LTP consolidation but do not address how modest patterned activity gives rise to dramatic changes in spine cytoarchitecture. Detailed descriptions of membrane receptor to cytoskeleton signaling in developing neurons have highlighted the roles of small GTPases (Kuhn et al., 2000). Yet, it is not known how these pathways contribute to the maintenance of adult dendritic spines or the production of synaptic plasticity, and evidence that they are engaged during LTP in adult brain has only recently been reported (Chen et al., 2007).

An important clue about mechanisms lies in the observation that endogenous adenosine is a potent, negative modulator

C.S. Rex and L.Y. Chen contributed equally to this paper.

Correspondence to Christopher S. Rex: crex@uci.edu

Abbreviations used in this paper: A1R, adenosine A1 receptor; ACSF, artificial cerebral spinal fluid; AMPAR, AMPA receptor; fEPSP, field excitatory postsynaptic potential; FXS, fragile X mental retardation syndrome; ir, immunoreactivity; JPK, jasplakinolide; Lat A, latrunculin A; LTP, long-term potentiation; PAK, p21-activated kinase; PPF, paired pulse facilitation; PSD, postsynaptic density; ROCK, RhoA kinase; str., stratum; TBS, theta burst stimulation.

The Rockefeller University Press $30.00
J. Cell Biol. Vol. 186 No. 1 85–97
www.jcb.org/cgi/doi/10.1083/jcb.200901084

of rapid consolidation. Reversal of LTP during its vulnerable period by hypoxia (Arai et al., 1990) or low frequency stimulation (Larson et al., 1993) is mediated by released adenosine. In this study, based on results obtained using adenosine as a probe, we report the first evidence that LTP induction sets in motion two independent signaling cascades, one that triggers actin polymerization and a second that contributes to the stabilization of the newly assembled filaments. The combined action of the two pathways is required for consolidation to reach completion. These findings point the way to a formal hypothesis regarding a fundamental feature of memory encoding and are directly relevant to discussions about the causes of mental retardation.

Results

Adenosine disrupts LTP consolidation by blocking actin polymerization in dendritic spines

Effects of adenosine on LTP and cytoskeletal reorganization were evaluated for field CA1 in adult rat hippocampal slices. Local application of 0.2 mM adenosine for 4 min, beginning 30 s after LTP induction by theta burst stimulation (TBS), caused a transient block of synaptic responses followed by a rapid recovery to the pre-LTP baseline (Fig. S1). The same treatment at 10 min after TBS failed to reverse LTP. Thus, adenosine fully reverses LTP in a time-dependent manner. We then labeled F-actin in situ with Alexa Fluor 568–phalloidin (Fig. 1 A and Video 1) to test the effects of adenosine on actin filament assembly in dendritic spines after LTP induction. Adenosine's effects on TBS-induced spine F-actin paralleled its actions on LTP: local application at 30 s but not 10 min after TBS blocked the threefold increase in the numbers of spines containing dense F-actin (Fig. 1 B). 0.2 µM of the selective adenosine A1 receptor (A1R) antagonist DPCPX (8-cyclopentyl-1, 3-dipropylxanthine) eliminated the suppressive action of adenosine at 30 s after TBS. These results accord with earlier findings (Kramar et al., 2006) and suggest that adenosine blocks the rapid stabilization of LTP by suppressing activity-induced cytoskeletal modifications.

We tested the aforementioned conclusion using jasplakinolide (JPK), a toxin which stabilizes newly formed actin filaments. JPK infusion caused a 40% reduction in synaptic responses without evident effect on paired pulse facilitation (PPF), suggesting that the toxin's actions are not a result of altered transmitter release probability (Fig. 1 C). JPK blocks AMPA (α-amino-3-hydroxyl-5-methyl-4-isoxazole-propionate) receptor (AMPAR) internalization in dissociated neurons (Zhou et al., 2001), but little is known about its effects on receptor cycling at adult synapses. Another study suggests that JPK's effect on actin stabilization slows the movement of glutamate receptors between synaptic and extrasynaptic membrane compartments (Ireland and Abraham, 2009). A bidirectional effect of this sort could slow the constitutive replacement of AMPARs without necessarily disrupting structural changes produced by TBS-driven filament assembly.

Field excitatory postsynaptic potentials (fEPSPs) were restored to pre-JPK levels by increasing the stimulus strength, and then TBS was applied. The magnitude of LTP induced by TBS (131.0 ± 2.6% of baseline) was slightly less in JPK-treated slices than that in untreated controls (145.0 ± 4.4%). This was not likely caused by disturbances of induction events because acute responses to TBS were not affected by JPK (Fig. S2), and expression of LTP at 1–2 min after TBS appeared normal (Fig. 1 C). Moreover, JPK did not reduce TBS-induced spine F-actin (Fig. 1 D). Adenosine infusions at 30 s after TBS transiently blocked transmission in JPK-treated slices but, in contrast to results obtained in control slices, failed to reverse LTP (Fig. 1, D and E).

Adenosine blocks TBS-induced cofilin phosphorylation

We investigated the possibility that adenosine exerts its disruptive influence on actin polymerization and LTP consolidation by interfering with the constitutively active actin depolymerizing protein cofilin, whose inactivation via phosphorylation is essential to cytoskeletal reorganization (Gungabissoon and Bamburg, 2003) and is associated with LTP (Chen et al., 2007). Hippocampal slices were immunolabeled and processed for deconvolution microscopy and reconstruction in three dimensions. Discrete cofilin-immunopositive (cofilin$^+$) structures (0.2–0.6 µm diameter) were present in large numbers in proximal CA1 stratum (str.) radiatum (Fig. 2 A) in association with similar-sized puncta immunopositive for PSD95, which is an integral postsynaptic density (PSD) protein. This agrees with evidence that cofilin is concentrated in spines in close proximity to excitatory synaptic junctions (Racz and Weinberg, 2006). Phospho-cofilin$^+$ (pCofilin$^+$) synapses had similar sizes and locations but were much less numerous (Fig. 2 B and Video 2).

We confirmed previous work (Chen et al., 2007) that LTP induction is followed by increases in the number of PSDs associated with dense levels of pCofilin (Fig. 2 C). Automated quantification of spine pCofilin and PSD95 immunoreactivity (ir) from slices in which LTP was recorded for 5 min allowed for analysis of colocalization across large numbers of synapses. More than 80% of pCofilin$^+$ elements were also PSD95$^+$ (n = 7,116 synapses from eight control slices). TBS caused an approximately threefold increase in pCofilin$^+$ PSDs (control vs. TBS: 3.2 ± 1.0/100 µm^3 vs. 11.7 ± 2.7/100 µm^3; n = 7–8; P = 0.01; Fig. 2 D) but had no effect on the total number of PSDs in the same slices (P = 0.4) or numbers of total (predominately unphosphorylated) cofilin$^+$ PSDs in different slices (n = 5; P = 0.6).

We tested whether the TBS-induced pCofilin effect is modified by adenosine. Brief (4 min) adenosine infusions to control slices reduced the number of pCofilin$^+$ synapses in CA1 str. radiatum by ∼30%, and this effect was completely blocked by the A1R antagonist DPCPX (Fig. 3 A). Moreover, adenosine applied at 30 s after TBS profoundly reduced the increase in pCofilin$^+$ synapses normally found after TBS (72 ± 15% vs. 273 ± 39% of control for adenosine vs. vehicle; n = 11 and 14; P < 0.0001). The potent block of activity-driven cofilin phosphorylation by adenosine was eliminated by DPCPX (Fig. 3 A) but was unaffected by 10 µM of the adenosine A2a receptor antagonist MSX3 (117 ± 24% of control + adenosine; P = 0.52). Because adenosine depressed basal pCofilin levels, we recalculated

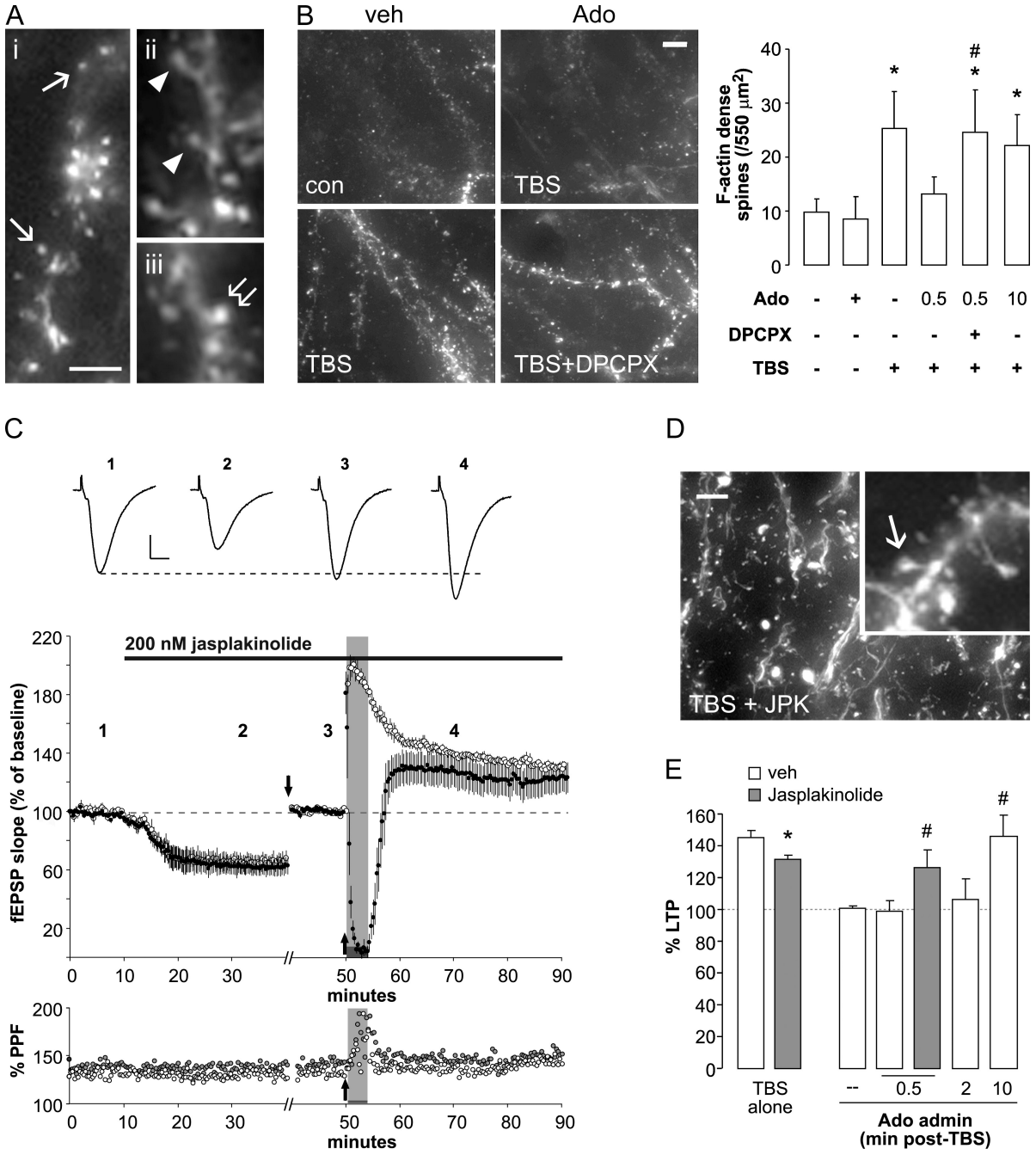

Figure 1. **Adenosine reverses LTP-associated actin polymerization via the A1R in a time-dependent manner.** (A) F-actin was labeled in situ with Alexa Fluor 568–phalloidin in the region of physiological recording in adult hippocampal slices. Photomicrographs show densely phalloidin-labeled spines (arrows; i). Labeled spines with clear necks (arrowheads; ii) and richly labeled mushroom spines (double arrow; iii) were often detected. (B) F-actin labeling in slices receiving control stimulation (con) or TBS followed by local infusion of vehicle (veh), adenosine (Ado), or adenosine in the presence of 0.2 μM DPCPX. The plot shows the quantification (means ± SEM) of phalloidin-labeled spines for slices receiving vehicle or adenosine at the indicated minutes after TBS (*, $P < 0.05$ vs. control; #, $P < 0.05$ vs. adenosine at 0.5 min after TBS). (C, top) Representative fEPSP traces at time points enumerated in the plot. Vertical bar, 0.5 mV; horizontal bar, 5 ms. (middle) Group fEPSP slopes for slices treated with JPK (solid horizontal line). Response amplitudes were returned to predrug levels by adjusting stimulus intensity (downward arrow); the gap in the x axis represents the time to stabilize the new baseline (<10 min). Slices receiving TBS alone (upward arrow; open circles) exhibited potentiation for >40 min. Slices receiving adenosine (gray shading) beginning 30 s after TBS (closed circles) returned to potentiated levels after washout. (bottom) PPF (percent amplitudes of pulse 2 vs. pulse 1) at 50 ms (gray circles) or 100 ms (open circles) interpulse intervals in a single case from plot immediately above. (D) In situ F-actin labeling in a slice receiving TBS in the presence of JPK. The arrow indicates a densely labeled spine. (E) Adenosine was applied at 0.5, 2, or 10 min after TBS. LTP is presented as mean percentage (±SEM) of baseline for the period from 10–20 min after vehicle or adenosine washout (*, $P < 0.5$ vs. vehicle/TBS alone; #, $P < 0.01$ vs. vehicle/0.5 min after TBS). (C and E) Dashed lines indicate baseline levels. Bars: (A [i], B, and D) 5 μm; (A [ii]) 3 μm; (A [iii] and D [inset]) 2 μm.

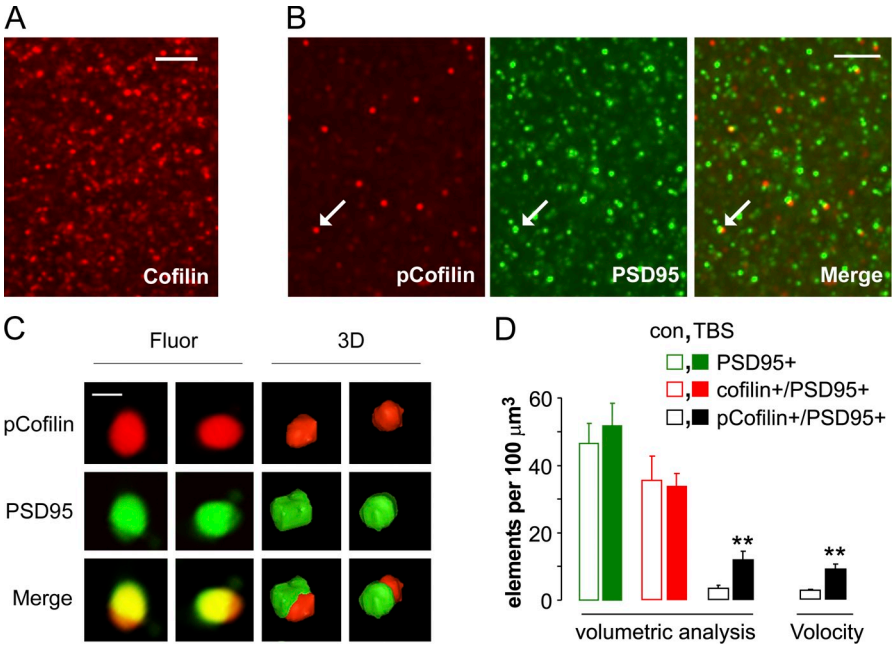

Figure 2. **3D reconstruction analysis of immunofluorescence.** (A) Deconvolution photomicrograph from proximal CA1 str. radiatum shows total cofilin$^+$ elements. (B) Images show localization of pCofilin$^+$ (left) and PSD95$^+$ (middle) elements in the same field (the arrows indicate overlapping structures). pCofilin$^+$ elements were of similar size and shape as total cofilin$^+$ elements (but less numerous). (C) Photomicrographs (Fluor) and volumetric reconstructions (3D) of a single synapse containing pCofilin ir and PSD95 ir displayed in 30° clockwise turns (left to right). (D) The plot shows numbers of immunolabeled spines (mean ± SEM) in the field of physiological recording for slices receiving control stimulation (con; open bars) or TBS (closed bars). Counts were made from 3D reconstructions. The plot shows separate quantification of total PSD95$^+$, double-labeled cofilin (cofilin$^+$/PSD95$^+$), and double-labeled pCofilin (pCofilin$^+$/PSD95$^+$) elements. The latter comparison was replicated using the Volocity measurement module. PSD95$^+$ elements associated with pCofilin ir represented <5% of the total PSD95$^+$ puncta in control slices. Slices receiving TBS showed approximately threefold more pCofilin$^+$/PSD95$^+$ colabeled elements versus controls (**, $P < 0.01$). Bars: (A and B) 5 µm; (C) 0.5 µm.

the effects of TBS as the percent change from the appropriate (adenosine treated or untreated) control group mean (Fig. 3 B). By this measure, TBS increased the number of pCofilin$^+$ PSDs by 173 ± 39% in untreated slices but only by 44 ± 16% in slices treated with adenosine ($P = 0.001$). The full effect of TBS was restored in adenosine-treated slices by preincubation with DPCPX (156 ± 64% of adenosine + DPCPX–treated control slices). Western blot analyses confirmed that adenosine infusion reduced basal pCofilin levels in control slices (vehicle vs. adenosine: 39.8 ± 4.2 vs. 26.3 ± 3.0 × 10^3 OD units; $n = 19$; $P = 0.01$; Fig. 3 C). Similar results were obtained when normalized to β-actin.

Trains of low frequency stimulation both release adenosine (Wall and Dale, 2007) and produce a time-dependent reversal of LTP (Larson et al., 1993); the latter effect is blocked by A1R antagonists. These observations raise the possibility that the aforementioned A1R effects on TBS-induced pCofilin can be engaged by repetitive synaptic activity. We tested this using a 3-min-long train of 5 Hz stimulation beginning 30 s after TBS, a treatment known to thoroughly disrupt LTP consolidation. The 5-Hz train completely blocked the increase in pCofilin$^+$ PSDs that normally occurs after TBS (TBS vs. TBS + 5 Hz: 243 ± 33% vs. 114 ± 12%; $n = 5$ and 11; $P < 0.001$; Fig. 3 D).

Adenosine does not block TBS-induced phosphorylation of p21-activated kinase (PAK)

In many cell types, cofilin phosphorylation is regulated by parallel signaling streams through the Rho GTPase effectors RhoA kinase (ROCK) and PAK. The latter is concentrated at synapses, regulates dendritic spine morphology, and is phosphorylated by TBS (Boda et al., 2004; Chen et al., 2007). Immunostaining for PAK3 in field CA1 produced punctate labeling resembling that for total cofilin; pPAK$^+$ structures were much less frequent and closely associated with PSDs (Fig. 4 A). Unexpectedly, local application of adenosine alone increased the number of pPAK$^+$ PSDs (444 ± 120% of control; $n = 11$ and 7; $P = 0.009$; Fig. 4 B). This result indicates that reductions in baseline levels of pCofilin by adenosine (Fig. 3) are not caused by a suppression of the PAK–LIM kinase–cofilin pathway.

TBS caused a sixfold increase in the number of pPAK$^+$ PSDs in control slices, and this effect was not attenuated by adenosine infusion beginning 30 s after TBS (Fig. 4 B). Recalculating the data as percent increase relative to baseline in adenosine-treated (no TBS) slices demonstrated a TBS-induced increase of 484 ± 89% in the number of pPAK$^+$ PSDs (Fig. 4 C). This value is not reliably different from the effect of TBS in untreated slices (636 ± 78%; $P = 0.2$).

The approximately fourfold increase in baseline pPAK$^+$ PSDs produced by adenosine was not accompanied by an equivalent change in Western blot analyses of hippocampal slice homogenates: pPAK band ODs were not significantly different for samples from treated versus untreated slices ($n = 18$; $P = 0.4$; Fig. 4, D and E). However, correcting values for within-lane actin levels uncovered a modest but reliable adenosine effect (0.90 ± 0.03 vs. 1.08 ± 0.07 fraction of control; $P = 0.02$). Overall, the pattern of results suggests that adenosine receptor activation causes translocation of pPAK to the synaptic compartment or that large extrasynaptic pools mask its effects at synapses in overall slice measures. In all, adenosine increases synaptic pPAK levels under control conditions but has little if any effect on increases in PAK phosphorylation associated with LTP induction.

Selective effects of adenosine on Rho GTPases

PAK and cofilin phosphorylation are regulated by Rho family small GTPases in many cell systems (Gungabissoon and Bamburg, 2003). Accordingly, we investigated the effects of

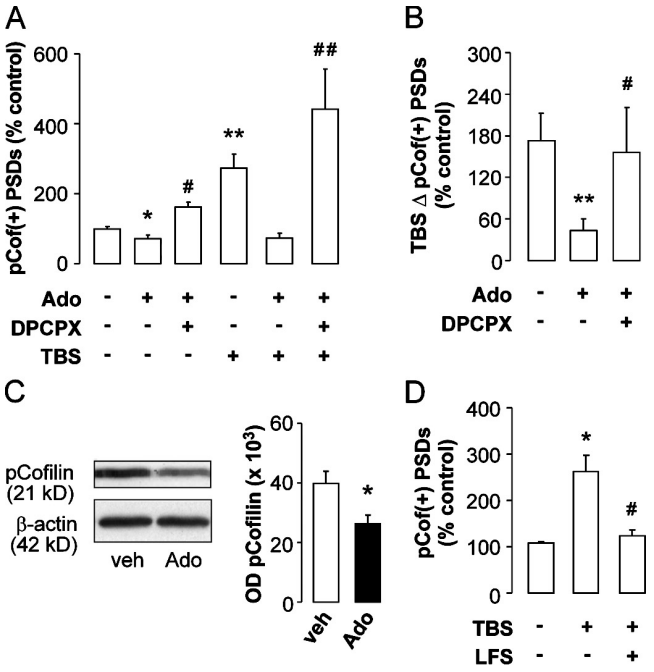

Figure 3. **Adenosine blocks phosphorylation of the F-actin–severing protein cofilin.** Hippocampal slices receiving TBS or control stimulation to the Schaffer collaterals were processed for double pCofilin (pCof) and PSD95 immunofluorescence. 0.2 mM adenosine (Ado) or vehicle (veh) was locally applied for 4 min beginning 30 s after TBS. (A) The plot shows mean numbers (±SEM) of pCofilin/PSD95 double-labeled puncta in the zone of physiological recording (*, P < 0.05; **, P < 0.01 vs. vehicle; #, P < 0.05; ##, P < 0.01 vs. adenosine alone). (B) Results from A expressed as difference between treatment and TBS + treatment effects (TBSΔ; mean ± SEM; **, P < 0.01 vs. vehicle; #, P < 0.05 vs. adenosine). (C) Western blots from tissue treated with adenosine or vehicle for 5 min; plot of group mean (±SEM) band ODs shows that adenosine decreased pCofilin levels (*, P < 0.05). (D) Low frequency stimulation (LFS) blocked TBS-induced increases in numbers of pCofilin⁺ PSDs (mean ± SEM; *, P < 0.05 vs. control; #, P < 0.05 vs. TBS).

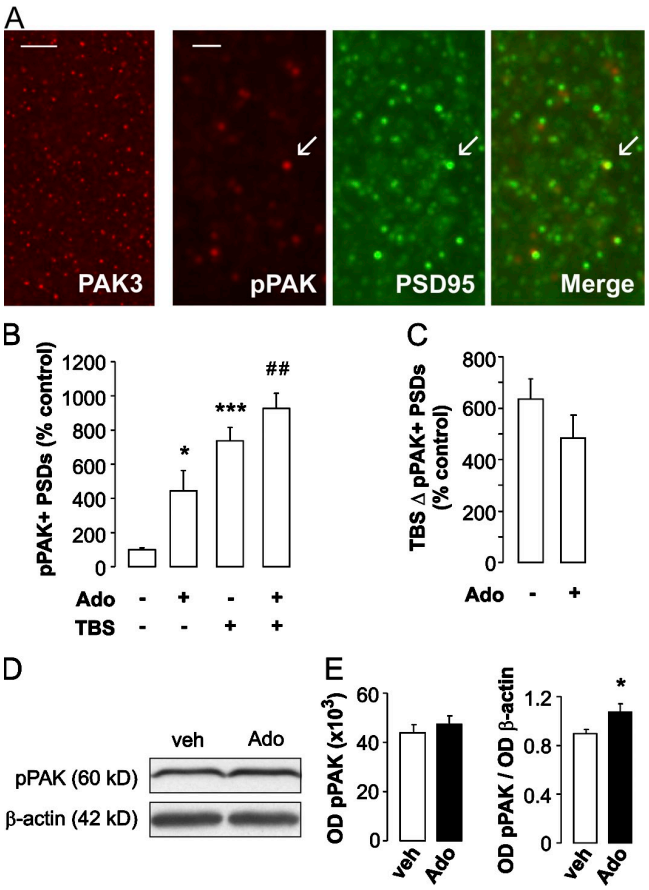

Figure 4. **Activity-induced PAK phosphorylation is not blocked by adenosine.** (A) Deconvolution images show total PAK3 ir (left) and the colocalization of pPAK1/2/3 and PSD95 (right panels) in proximal CA1 str. radiatum. The arrows indicate a double-labeled element. (B) Quantification (mean ± SEM) of pPAK⁺ PSDs shows that adenosine (Ado) significantly increased the numbers of pPAK⁺ PSDs (n = 7–11; *, P < 0.05 vs. control). TBS followed by adenosine 30 s later increased pPAK⁺ PSDs above values in adenosine alone slices (n = 11; ***, P < 0.001 vs. control; ##, P < 0.01 vs. adenosine). (C) Results from B presented as the difference between TBS + treatment and treatment alone group values (TBSΔ; mean ± SEM). (D) Western blots from slices treated with adenosine or vehicle (veh) for 5 min (same slices as in Fig. 3 C). (E) Plots show raw band ODs (left) or the same measure normalized to β-actin (right; means ± SEM; *, P = 0.02). The latter measure exposed an adenosine-induced increase in levels of pPAK. Bars: (A [left]) 10 μm; (A [right]) 5 μm.

adenosine on Rho-GTPase activity in adult hippocampus with pull-down assays that purify active (GTP bound) RhoA or Cdc42/Rac. 0.2 mM adenosine treatment for 5 min markedly reduced levels of GTP-bound RhoA (P = 0.009), produced a modest inhibition of Cdc42 activity (P = 0.016), and had no detectable effect on Rac activity ($n \geq 10$; P = 0.07; Fig. 5, A and B). Adenosine did not affect total levels of the three GTPases. These findings constitute the first evidence that adenosine differentially regulates Rho GTPases in adult hippocampus and suggest that its reversal of LTP and activity-driven cofilin phosphorylation involves suppression of RhoA. From this and the finding that TBS triggers both PAK and cofilin phosphorylation, we predicted that synaptic potentiation would activate both Rac and RhoA. It is difficult to apply pull-down assays in conventional CA1 LTP experiments because only a small fraction of the synaptic population is engaged (Chen et al., 2007). Accordingly, we used a broadly acting, chemically induced form of potentiation that bears several resemblances to LTP (Roth-Alpermann et al., 2006); as predicted, this was accompanied by a significant activation of RhoA and Rac (n = 5–8; P < 0.05) as well as pPAK and pCofilin (Fig. S3).

The aforementioned results suggest that adenosine blocks cofilin phosphorylation via the RhoA effector ROCK, which activates LIM kinase and in turn phosphorylates cofilin. If so, ROCK inhibitors should, like adenosine, reduce both baseline and TBS-induced pCofilin. We tested this by infusing hippocampal slices with 0.1 μM of the potent and selective ROCK inhibitor H1152 for 30 min. H1152 reduced pCofilin levels to 41 ± 6% of control values in Western blots (n = 17; P < 0.0001) without measurable effect on basal pPAK levels (Fig. 5 C).

As expected from the aforementioned results, H1152 applied alone caused a substantial reduction in baseline numbers of pCofilin⁺ PSDs (48 ± 29% of vehicle; n = 6 and 5; P = 0.01; Fig. 5 D). The ROCK inhibitor also offset the increase in pCofilin⁺ PSDs normally seen after LTP induction. We estimated the magnitude of this suppression by calculating the percent increase produced by TBS in the presence of the ROCK inhibitor: the increment with TBS (TBSΔ: 35 ± 25%) was substantially smaller in the presence of H1152 than in untreated slices (97 ± 15%;

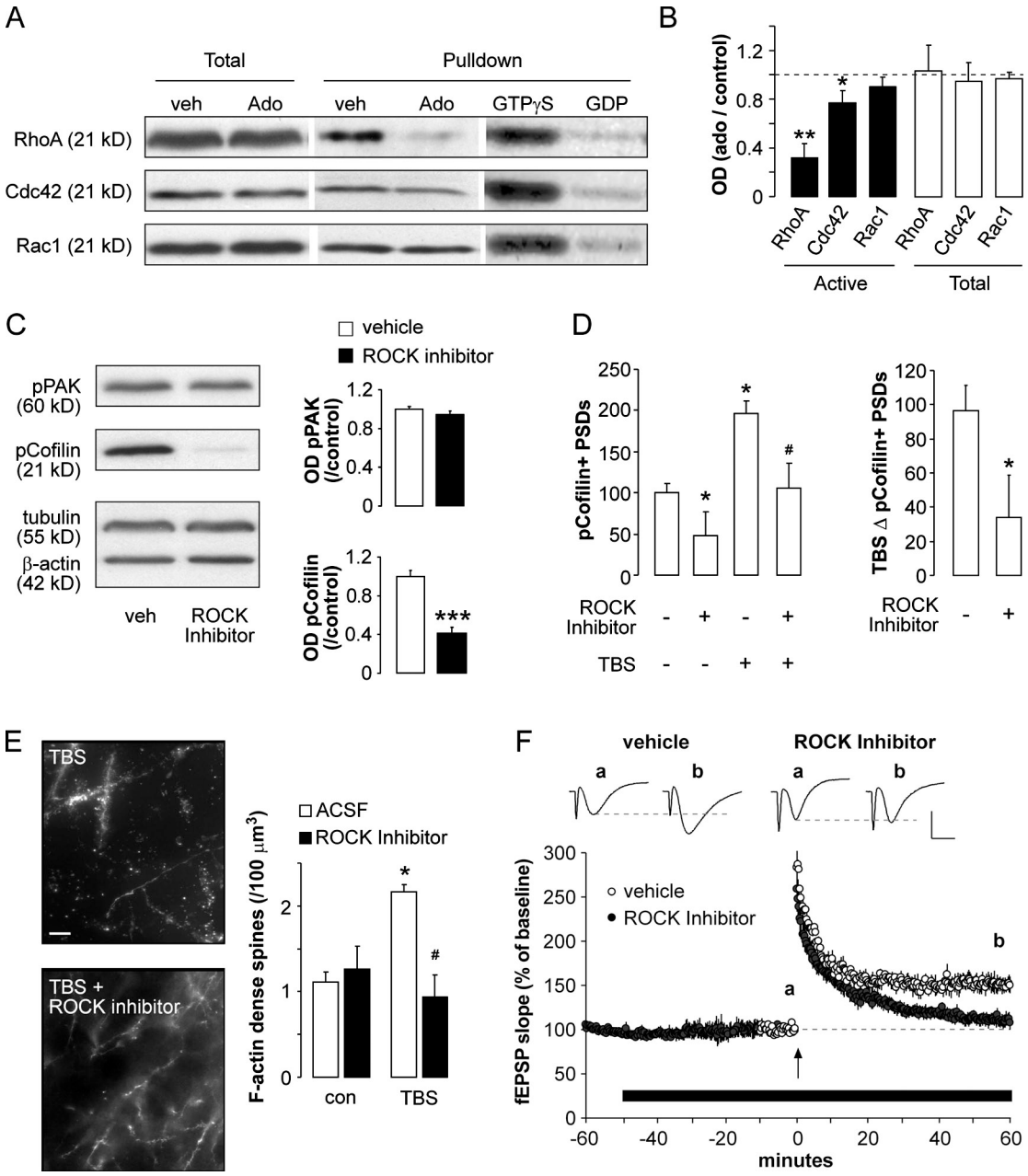

Figure 5. **RhoA signaling is necessary for stable expression of LTP.** (A) Western blots from vehicle (veh)- or adenosine (Ado)-treated slices probed with antisera for total RhoA, Cdc42, or Rac1 (left) or (in the same samples) processed by pull-down assay (middle) using GST-Rhotekin (for RhoA)– or GST-PAK (for Cdc42 and Rac1)–binding domains. (B) Group mean (±SEM) band OD measures from pull-downs (Active) or total protein measures for the indicated GTPases are expressed as adenosine treatment/control (*, $P < 0.05$; **, $P < 0.01$ vs. vehicle). (C) Western blot and plots of band densities show pPAK and pCofilin levels in slices treated with 0.1 μM of the ROCK inhibitor H1152 for 30 min or vehicle; H1152 selectively suppressed pCofilin ir (mean ± SEM; ***, $P < 0.001$ vs. vehicle). (D, left) Slices were treated with H1152 for 30 min before TBS and harvested 7 min after TBS for immunofluorescence; numbers of pCofilin$^+$ PSDs in the zone of physiological recording are shown (*, $P < 0.05$ vs. vehicle/control; #, $P < 0.05$ vs. H1152 alone). (right) Object counts, presented as the mean (±SEM) difference between TBS + treatment and treatment alone groups (TBSΔ; *, $P < 0.05$), show that H1152 blocks the TBS effect. (E) Images show in situ F-actin labeling in slices receiving TBS alone or TBS + ROCK inhibitor. Group mean (±SEM) numbers of phalloidin-labeled spines/100 μm^3 for TBS- and control-stimulated (con) slices in the absence (ACSF) or presence of H1152 are shown (*, $P < 0.05$ vs. control; #, $P < 0.05$ vs. ACSF-TBS). (F) Slices were treated with H1152 (solid horizontal line) for 50 min before TBS (arrow). H1152-treated slices (closed circles) showed normal initial potentiation compared with vehicle controls, but LTP failed to stabilize. (top) Baseline (left) and 60-min post-TBS (right) fEPSP traces. Vertical bar, 1 mV; horizontal bar, 10 ms. (B and F) Dashed lines indicate baseline levels. Bar, 5 μm.

$P = 0.04$; Fig. 5 D). H1152 also blocked the TBS-induced increase in spines with dense F-actin content (TBS vs. TBS + H1152: 2.2 ± 0.1 vs. 0.9 ± 0.3 phalloidin-labeled spines/100 μm^3; $n = 5–6$; $P = 0.001$; Fig. 5 E). As with adenosine, the ROCK inhibitor did not alter baseline numbers of phalloidin-labeled spines ($P = 0.6$). These results indicate that TBS inactivates cofilin and thereby promotes actin filament assembly by stimulating adenosine-sensitive RhoA-ROCK signaling.

An important prediction from the aforementioned argument is that ROCK inhibition will disrupt LTP consolidation. Studies

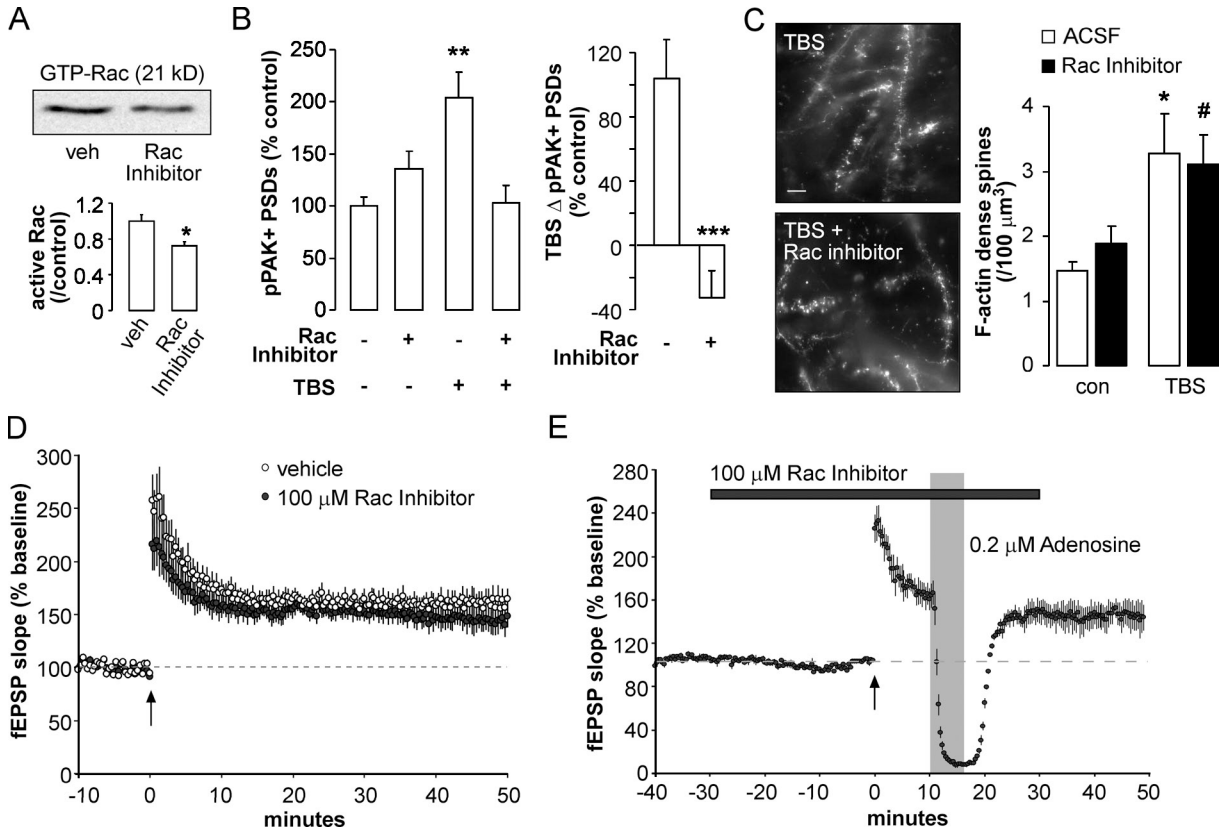

Figure 6. **Inhibition of activity-driven PAK phosphorylation does not block LTP or activity-induced spine F-actin.** (A) Hippocampal slices were treated with 0.1 mM of the Rac inhibitor NSC23766 or vehicle (veh) for 1 h and processed for Rac pull-down assay. Representative blot and group mean (±SEM) values show that NSC23766 reduced active Rac1 levels by >30% (*, $P < 0.01$ vs. vehicle). (B) Slices were treated for 30 min with the Rac inhibitor before TBS and harvested 7 min after TBS for immunofluorescence. NSC23766 did not affect baseline levels of pPAK+ PSDs when applied alone but did block the effects of TBS on this measure (**, $P < 0.01$ vs. control). The right plot shows mean (±SEM) values of the same measures expressed as the difference between TBS + treatment and treatment alone groups (***, $P < 0.001$ vs. vehicle). (C) Images show in situ F-actin labeling in slices receiving TBS alone or TBS + NSC23766. The plot shows group mean (±SEM) numbers of labeled spines/100 μm^3 (*, $P < 0.01$ vs. ACSF; #, $P = 0.01$ vs. NSC23766 alone). con, control. (D) The Rac inhibitor was applied to slices for 30 min before TBS (arrow) and remained throughout recording; no effects on LTP were observed in comparison to vehicle control slices. (E) LTP induced by TBS (arrow) in the presence of the Rac inhibitor did not show reversal after 6-min local adenosine treatment (gray shading) beginning 10 min after TBS. (D and E) Dashed lines indicate baseline levels. Bar, 5 μm.

using Y-type inhibitors have described mixed results (O'Kane et al., 2004; Wang et al., 2005); the more selective H1152 (Sasaki et al., 2002) has only been tested in the dentate gyrus, where it blocked LTP (Huang et al., 2007). We measured LTP in slices infused with concentrations of H1152 (0.1 μM) sufficient to block cofilin phosphorylation. The inhibitor had no discernible effects on input–output relationships or PPF of synaptic responses (Fig. S4) and did not alter baseline responses (Fig. 5 F). LTP induced in the presence of H1152 failed to stabilize: the initially potentiated responses returned to near baseline levels within 60 min (vehicle vs. H1152: 151 ± 9% vs. 111 ± 7% of baseline; $n = 4$ and 7; $P = 0.005$). In particular, the ROCK inhibitor appeared to exert its influence on consolidation because it had no effect on the size of burst responses used to induce LTP (Fig. S4) and did not change initial potentiation (vehicle vs. H1152: 284 ± 9% vs. 248 ± 22% for 0–1 min after TBS; $P = 0.2$).

Rac-PAK signaling is required for LTP stabilization

The aforementioned results lead to the hypothesis that TBS sets in motion two parallel signaling cascades, one (RhoA-ROCK-cofilin) that is sensitive to adenosine and another (Cdc42/Rac-PAK-?) that is not. After establishing that RhoA signaling is linked to TBS-induced actin polymerization, we investigated the effects of disrupting Rho GTPase–PAK signaling on the expression and stabilization of LTP. Given the absence of widely tested Cdc42 inhibitors, we used the highly selective small molecule inhibitor NSC23766 to block Rac GTPase activity (Gao et al., 2004). This compound interferes with binding of Rac-specific guanine exchange factors without disrupting Cdc42 or RhoA GTP/GDP exchange.

Treatment with 0.1 mM of the Rac inhibitor for 1 h reduced levels of GTP-Rac by >30% ($n = 4$–5; $P = 0.04$; Fig. 6 A) without detectably changing PAK or cofilin phosphorylation (Fig. S5). NSC23766 has similarly little effect on basal levels of pPAK in Schwann cells, suggesting that Rac may not constitutively activate this effector (Thaxton et al., 2007). The inhibitor also did not reduce basal synaptic pPAK in slices (Fig. 6 B). However, it did completely block TBS-induced increases in numbers of pPAK+ PSDs (TBS vs. TBS + NSC23766: 204 ± 25% vs. 103 ± 16%; $n = 6$; $P = 0.002$). Despite this, the Rac inhibitor did not disrupt TBS-induced increases in spines containing dense F-actin

(TBS vs. TBS + NSC23766: 3.3 ± 0.6 vs. 3.1 ± 0.4 spines/100 μm^3; n = 9; P = 0.47; Fig. 6 C).

We then tested whether Rac-PAK signaling contributes to LTP. Infusion of the inhibitor for 30 min before TBS did not affect baseline physiology or initial expression and subsequent maintenance of LTP (P > 0.6 vs. vehicle; Fig. 6 D). We then asked whether NSC23766 affects processes that render LTP resistant to disruption. Adenosine infusion beginning 10 min after TBS, a time point at which it does not affect LTP (Fig. 1 A), was also without effect on potentiation in Rac inhibitor–treated slices (Fig. 6 E). These findings indicate that blocking TBS-induced phosphorylation of synaptic PAK does not prolong the period over which LTP is vulnerable to adenosine.

We next tested for a contribution of Rac/PAK on the stabilization of TBS-induced spine F-actin. Newly assembled actin filaments in various cell systems commonly remain in a dynamic state ("treadmilling") until stabilized by various specialized protein systems. Latrunculin A (Lat A) disrupts treadmilling by preventing the addition of actin monomers to growing filaments, and this produces sizeable alterations to AMPAR currents at sufficient concentrations (>5 μM; Kim and Lisman, 1999; Zhou et al., 2001). Therefore, we used a dose (0.2 μM) that blocks LTP consolidation when applied before or shortly after TBS without evident effect on basal synaptic physiology (Krucker et al., 2000). We confirmed this using 4-min-long local infusions of Lat A to slices: infusions initiated 30 s or 2 min but not 10 or 30 min after TBS caused potentiated responses to return to near baseline within 90 min (Fig. 7 A). Accordingly, Lat A applied at the early (30 s or 2 min) but not late (10 or 30 min) time points also disrupted the spine F-actin increases typically observed after TBS. This finding provides a first demonstration that the F-actin assembled within spines after TBS shifts from a dynamic to a stable state over a period of several minutes and strongly suggests that this transition is the event underlying the consolidation of LTP.

LTP's resistance to Lat A at 10 or more minutes after TBS was not overcome by longer infusions: 80-min Lat A applications initiated 10 min after LTP induction were ineffective at reversing potentiation (Fig. 7 B), suggesting that, under normal conditions, TBS-induced filaments are fully stabilized by this point. In contrast, Lat A infusions beginning 10 min after TBS caused potentiated responses to gradually decay back to their pre-TBS baselines in slices pretreated with 0.1 mM NSC23766 for 30 min. The difference in Lat A's effects on percent LTP at the conclusion of recording in untreated (51 ± 4%) and Rac inhibitor–treated (10 ± 7%) slices was highly significant (n = 8; P = 0.001). Notably, Lat A caused no changes to unpotentiated responses (control pathway) recorded from the same slices infused with the Rac inhibitor. In parallel experiments, we pretreated slices with 0.1 mM NSC23766 for 30 min or vehicle, induced LTP, infused 0.2 μM Lat A 10 min later, and then labeled F-actin in situ with phalloidin. Lat A significantly reduced the numbers of F-actin–dense spines in NSC23766-treated but not vehicle-treated slices (Fig. S5), confirming that Rac inhibition extends the post-LTP induction period over which TBS-induced spine F-actin requires continuous filament assembly.

If NSC23766 acts on Rac-PAK signaling to prolong the period during which Lat A reverses LTP, a selective inhibitor of PAK should reproduce its effects. To test this point, we used a small molecule, IPA-3, that directly and noncompetitively inhibits Group I PAK activity (i.e., PAK1–3; Deacon et al., 2008). 2 μM of the PAK inhibitor applied to slices for 1 h, at a concentration reported to block PAK1 activity without affecting 200 related kinases, blocked 50% of PAK phosphorylation at Thr423 (n = 6; P = 0.02 vs. control; Fig. 7 C). This catalytic domain site concludes a serial autophosphorylation chain triggered by GTPase binding (i.e., Cdc42 or Rac) and therefore represents one of the final modifications required for PAK to carry out its kinase activity (Chong et al., 2001). However, it did not block phosphorylation at the initial Ser141 autophosphorylation site within the regulatory domain (n = 6; P > 0.05 vs. control; Fig. 7 C). This result is expected from the inhibitory mechanism of IPA-3, which is believed to prevent PAK activity by stabilizing the kinase in a semi-open, catalytically inactive conformation (Deacon et al., 2008).

Slices incubated for 1 h with 2 μM IPA-3 showed no overt disturbances to baseline synaptic responses (Fig. 7 D). LTP appeared normal in the majority (78%) of inhibitor-treated cases, and we used these to challenge its stability. 0.2 μM Lat A infusions, initiated at 30 min after TBS and continued throughout recording, caused the potentiated responses to gradually decay back to their preinduction baseline values (the percentage of LTP at 2.5 h after induction was 105 ± 8%; n = 7; P = 0.6 vs. baseline; Fig. 7 D). Collectively, the aforementioned findings point to the presence of TBS-driven Rac-PAK signaling that, in spines, is insensitive to adenosine but critical for the stabilization of LTP-related cytoskeletal changes.

Discussion

Multiple lines of evidence indicate that adenosine, released during LTP induction, acts as a negative modulator of processes that stabilize recently generated synaptic potentiation. We found that extracellular adenosine, acting through A1Rs, blocks TBS-induced actin polymerization when applied shortly after stimulation. That actin polymerization is the central event underlying LTP's initial window of vulnerability is supported in this study by the demonstration that TBS-induced spine actin polymerization and synaptic potentiation exhibit similar patterns of vulnerability to Lat A, which prevents filament assembly. This argument predicts that, absent its potent influence on actin polymerization, adenosine would have no effect on LTP stabilization. We confirmed this by showing that the actin filament stabilizer JPK allowed LTP consolidation to go to completion despite the presence of adenosine. This accords with recent evidence that JPK can block reversal of late-phase LTP (Messaoudi et al., 2007).

The question then became one of how extracellular adenosine interferes with F-actin assembly in dendritic spines. We confirmed our previous finding (Chen et al., 2007) that LTP induction is followed by rapid phosphorylation of the actin-severing protein cofilin. Phosphorylation inactivates cofilin by preventing its binding to actin filaments (Gungabissoon and Bamburg, 2003) and thus promotes actin polymerization and filament

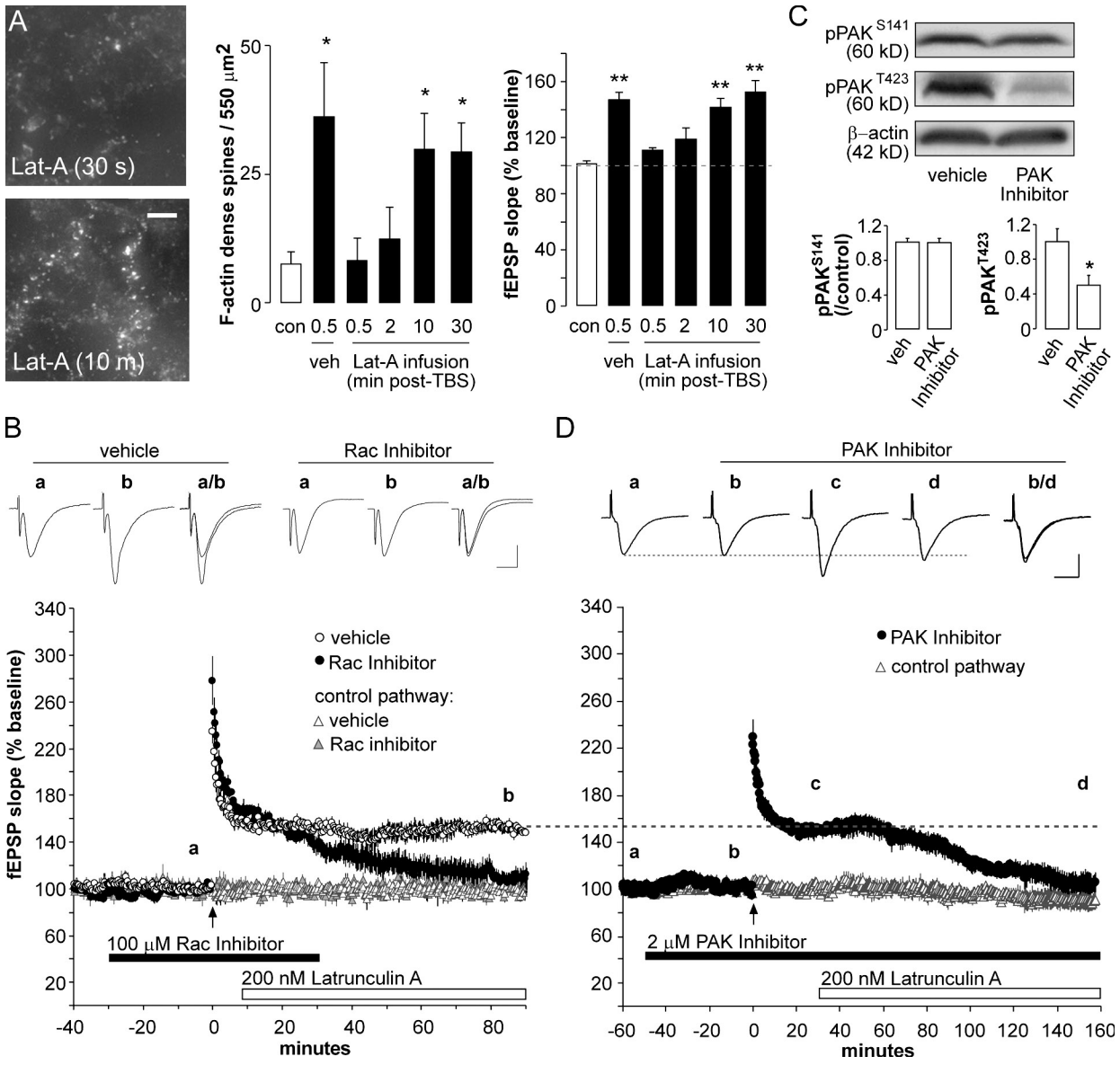

Figure 7. **Inhibition of Rac-PAK signaling extends the period over which actin filament assembly is required for LTP.** Stimulation was applied to Schaffer collateral afferents to hippocampal field CA1b. (A) Slices labeled for F-actin after 4-min local infusion of 0.2 μM Lat A. (left) Images show that Lat A blocked increases in phalloidin-labeled spines when applied 30 s but not 10 min after TBS. (middle) The plot shows F-actin–labeled spine counts (mean ± SEM) from slices treated with vehicle (veh) at 30 s after TBS or with Lat A initiated at the time points indicated (*, $P < 0.05$ vs. control). (right) The plot shows mean LTP magnitude (percent fEPSP slope measured 80–90 min after TBS vs. baseline) from experiments in which slices were treated locally with Lat A or vehicle for 4 min beginning at the time points indicated (**, $P < 0.01$ vs. respective control pathways). Measures for untreated, unstimulated (control [con]) slices are also shown. The dashed line indicates baseline level. (B) Prolonged Lat A bath infusion (open horizontal line), timed to hit slices at 10 min after TBS (arrow), did not disrupt LTP when applied alone (with vehicle) but blocked the stable maintenance of LTP in the presence of the Rac inhibitor NSC23766 (closed horizontal bar). A second control pathway (triangles) not receiving TBS was unaffected by drug manipulations. (top) Representative fEPSP traces collected at time points indicated in the plot. (C) Western blots from slices incubated with 2 μM of the Group I PAK–specific inhibitor IPA-3 for 1 h and probed for $pPAK^{S141}$ or $pPAK^{T423}$. β-Actin bands shown were generated from the stripped PAK^{T423} blot. Plots show group mean (±SEM) band densities as a fraction of vehicle controls (*, $P < 0.05$ vs. vehicle). (D) Slices incubated for 50 min with 2 μM IPA-3 (closed horizontal bar) before TBS (arrow; TBS pathway shown as closed circles) exhibited stable LTP of typical magnitude (dashed line), but Lat A washed in at 30 min after TBS caused potentiation to decay to baseline levels within 2 h. The unstimulated control pathway (open triangles) was unaffected by drug manipulations. (top) Representative fEPSP traces from the time points indicated. (B and D) Vertical bar, 1 mV; horizontal bar, 10 ms. Bar, 5 μm.

loading (Niwa et al., 2002; Thirone et al., 2009). Adenosine, applied after the initial expression of LTP and acting via A1Rs, completely suppressed the three- to fourfold increase in $pCofilin^{+}$ synapses produced by TBS. Low frequency stimulation, which blocks actin polymerization and LTP in an A1R-dependent fashion, also interfered with TBS-induced cofilin phosphorylation. These results demonstrate that A1R activation either blocks phosphorylation or greatly accelerates dephosphorylation of synaptic cofilin and thereby presumably increases the net activity of the protein. Therefore, they describe a mechanism through which adenosine prevents the actin polymerization needed for LTP stabilization.

Adenosine's actions on LTP-related actin signaling were surprisingly selective; after TBS, adenosine infusions did not affect the marked increases in the number of $pPAK^+$ synapses induced with LTP. LIM kinase is directly activated by PAK, and this action mediates PAK's regulation of cofilin (Bokoch, 2003). We previously proposed that TBS-induced cofilin phosphorylation in spines is regulated in this manner (Chen et al., 2007), but the present results argue against this idea and suggest instead that LTP induction initiates parallel signaling pathways, one of which goes through ROCK to cofilin and a second that involves PAK.

Rho GTPases, which translate transmembrane signaling to the actin cytoskeleton, are a logical starting point for analyses of upstream mediators of adenosine's differential actions on LTP consolidation events. In this study, we show that an NMDA (*N*-methyl-D-aspartate) receptor–dependent, chemically induced synaptic potentiation robustly activates RhoA and Rac, effects which are in accord with evidence that Rho GTPases are activated by Ca^{2+} influx through NMDA receptors (Semenova et al., 2007). Rho GTPase activity may also be driven by other factors (e.g., neurotrophins) released by TBS and known to produce effects through these enzymes (Gehler et al., 2004). Adenosine caused a profound inhibition of RhoA activity, a modest suppression of Cdc42, and no change in Rac activity. This pattern fits well with the effects of adenosine on PAK and cofilin because PAK is an effector for Cdc42 and Rac, whereas RhoA, acting through ROCK, drives cofilin phosphorylation (Bokoch, 2003). The results obtained in adult brain slices in this study may be a reflection of a developmentally conserved system because growth cone collapse and expansion are regulated by opposing Cdc42/Rac and RhoA activities (Huber et al., 2003). Moreover, this pathway distinction appears to persist at least through the early development of dendritic spines (Tashiro et al., 2000; Carlisle et al., 2008) and matches recent evidence that adenosine's actions on pituicyte morphology require RhoA but not Rac activity (Rosso et al., 2007). In the latter system, evidence suggests that signaling through the A1R inhibits RhoA via G protein regulation of a GTPase activating protein.

That adenosine increases baseline PAK phosphorylation while modestly depressing PAK's upstream activator Cdc42 is not entirely unexpected. There are multiple routes (e.g., Rac and sphingosine) for PAK activation, and one or more of these may be downstream from the A1R. But the key result with regard to LTP is that TBS-driven synaptic PAK phosphorylation is unaffected by adenosine. Thus, the transient activation of Rac-PAK signaling during LTP induction is likely to progress without being significantly influenced by adenosine.

The diverse adenosine results described in the previous paragraphs help to clarify the signaling pathways used by patterned afferent activity to reorganize the spine cytoskeleton and stabilize an otherwise transient potentiation of synaptic responses. As discussed, TBS-driven cofilin phosphorylation, likely an essential step for triggering actin polymerization within spines, appears to involve an adenosine-sensitive, RhoA-initiated signaling cascade rather than Cdc42/Rac-PAK–LIM kinase signaling. In accord with this, a ROCK inhibitor, at concentrations that had no effect on pPAK, thoroughly suppressed

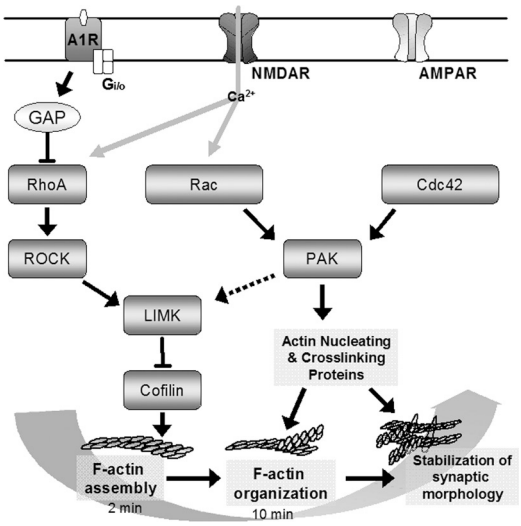

Figure 8. **Schematic of processes regulating cytoskeletal dynamics during LTP stabilization.** The proposed model shows signaling cascades that regulate distinct stages of dendritic spine actin reorganization. Activity-driven RhoA to cofilin signaling, leading to F-actin assembly, is rapid (~2 min) and A1R sensitive. Evidence from other systems suggests that A1R inhibits RhoA through a GTPase-activating protein (GAP). Parallel activation of PAK via Rac is adenosine insensitive and influences later (>10 min) LTP consolidation events. The dashed PAK to LIM kinase (LIMK) arrow denotes signaling, shown in neurons and other cell systems, that does not appear to be involved in synaptic potentiation or its concomitant actin polymerization. Rather, results in this study suggest that LTP-related PAK signaling regulates proteins involved in higher order organization of the spine cytoskeleton. The independence of the described signaling pathways and their functional roles in LTP suggest that activity-induced cytoskeletal reorganization has distinct and sequential stages involving RhoA and then Rac signaling. NMDAR, NMDA receptor.

TBS-induced increases in $pCofilin^+$ synapses and caused LTP to gradually decay back to baseline. In contrast, inhibition of Rac or PAK activity failed to produce the type of decremental LTP found with any of several treatments that block actin polymerization. This is consistent with the finding that suppression of PAK activity by overexpressing its inhibitory subunit does not detectably affect the decay rate of hippocampal LTP (Hayashi et al., 2004). In all, the results indicate that TBS sets in motion two signaling cascades, one of which leads to the actin filament assembly needed for LTP consolidation and another which has different functions (Fig. 8).

The present experiments provide evidence that activation of Rac-PAK signaling in synapses is part of the system whereby cytoskeletal changes needed to consolidate LTP are stabilized. Results in this study show that disruption of activity-induced actin polymerization by Lat A is time dependent relative to TBS, suggesting that the newly formed actin polymers cease treadmilling, an action typically involving filament capping, cross-linking, or nucleating proteins (Cooper and Sept, 2008). This idea is supported by evidence that PAK regulates proteins that support the filament branch nucleator Arp2/3, including cortactin and WAVE (Takahashi and Suzuki, 2009; Webb et al., 2006). In line with this, this study showed that inhibition of Rac or PAK prolonged the period over which LTP remains vulnerable to disruption by disassembly of dynamic filaments by latrunculin.

The evidence that Rac-PAK signaling is critical to stabilization as opposed to assembly events occurring 10–15 min after TBS does not preclude a role in later protein synthesis–dependent stages of LTP. Recent work suggests that latrunculin-sensitive changes in the spine cytoskeleton link synaptic activity to local protein synthesis (Smart et al., 2003; Sacktor, 2008), whereas knockout mouse experiments indicate that loss of PAK3 or WAVE selectively impairs late-phase, presumably protein synthesis dependent, LTP (Meng et al., 2005; Soderling et al., 2007). Thus, it is not unlikely that Rac-PAK signaling helps shape translational responses to LTP induction.

It is of interest that portions of the membrane receptor to cytoskeleton signaling machinery identified in the present work have been implicated in disorders of memory and cognition. Mutations disrupting gene products that regulate or transduce Rho GTPase activity are associated with mental retardation (van Galen and Ramakers, 2005). Moreover, abnormalities in Rac-PAK signaling may contribute to the fragile X mental retardation syndrome (FXS) phenotype (Linseman and Loucks, 2008). Actin remodeling is disturbed in a mouse model of FXS, and suppression of PAK activity with a dominant-negative transgene reduces FXS-related structural and functional abnormalities (Hayashi et al., 2007). Our results suggest that perturbations to Rac-PAK signaling will be accompanied by relatively discrete changes to synaptic operations in adult brain and, in particular, should leave baseline transmission as well as the induction and early expression of LTP intact. Conversely, mental retardation–related mutations that involve proteins acting on RhoA (e.g., oligophrenin 1) would be expected to have more potent effects on synaptic plasticity.

Materials and methods

All procedures were conducted in accordance with guidelines of the National Institutes of Health and the Institutional Animal Care and Use Committee of the University of California.

Electrophysiology

350-µm transverse hippocampal slices were prepared from 4–8-wk-old male Sprague Dawley (Harlan) rats in ice cold artificial cerebral spinal fluid (ACSF) containing 124 mM NaCl, 3 mM KCl, 1.25 mM KH_2PO_4, 5 mM $MgSO_4$, 26 mM $NaHCO_3$, 3.4 mM $CaCl_2$, and 10 mM dextrose using a vibroslicer (VT1000; Leica). Slices were maintained in an interface recording chamber (at 32°C with 95% O_2/5% CO_2) with constant 60–70 ml/min ACSF perfusion (Rex et al., 2007). Field electrophysiology was performed using two bipolar stimulating electrodes (65-µm twisted nichrome wire) placed in mid-proximal str. radiatum of CA1a and CA1c to stimulate independent populations of synapses recorded with a glass electrode (2 M NaCl) in CA1b (Chen et al., 2007). Baseline responses were set at 40–50% of maximum spike-free fEPSPs. For JPK experiments, responses were set at 30% of the maximum. LTP was induced by TBS (10 bursts of four pulses at 100 Hz with 200-ms interburst intervals). For some preparations, one pathway remained unstimulated as a control pathway. fEPSP slope values in figures and text are measured as 10–90% fall and are normalized to the 10 min before drug infusion or TBS. Input/output (stimulation duration vs. fEPSP amplitude) was performed as 10–20-µs duration steps and repeated three times for each step. PPF was measured as the percent fEPSP amplitude change between successive pulses tested at 10–100-ms interpulse intervals (repeated three times for each interval). For continuous assessment of PPF, single pulse test stimulation was replaced by paired test pulses (fEPSP slopes measured from responses to the first pulse only). Slices used for microscopic analysis were harvested 7 min after TBS and fixed in 4% PFA in 0.1 M of sodium phosphate buffer. *n* values represent slices/group.

Drugs

Adenosine (EMD), DPCPX (Tocris), JPK (Invitrogen), H1152 (EMD), Lat A (Invitrogen), and 1,1′-disulfanediyldinaphthalen (IPA-3; Sigma-Aldrich) were prepared in DMSO; MSX3 (3-[3-hydroxypropyl]-8-[3-methoxystyryl]-7-methyl-1-propargylxanthine; Sigma-Aldrich) and NSC23766 (Tocris) were prepared in double-distilled H_2O. Compounds were diluted in ACSF (<0.1% DMSO) and applied to the bath via perfusion line or local infusion (0.2 ml/min) using a glass micropipette (tip diameter ~25 µm; concentrations estimated after dilution in bath) controlled by a motorized injection pump (model 341B; Sage Instruments; Rex et al., 2007).

In situ labeling of F-actin

Alexa Fluor 568–phalloidin (6 µM in pipette; Invitrogen) was applied to slices (four 3-min intervals) beginning 15 min before TBS or drug infusion. Slices were collected 7–15 min after TBS or as stated and processed for microscopy as described in Deconvolution microscopy and quantification of synaptic structures. Labeling was quantified using in-house software (Rex et al., 2007). For tests using local Lat A application, phalloidin was applied (four 3-min intervals) beginning 20 min after the removal of the drug. Phalloidin applied after TBS produces comparable results with pre-TBS applications (Rex et al., 2007). Unless otherwise stated, values in the figures and text are presented per 550 µm^2 from collapsed 20-µm z stacks. Values presented per unit volume (100 µm^3) represent images processed and analyzed as described in Deconvolution microscopy and quantification of synaptic structures.

Immunocytochemistry

Fixed slices were sectioned (20 µm), slide mounted, and processed using a primary antisera cocktail of mouse anti-PSD95 (Thermo Fisher Scientific) with rabbit antisera to pPAK1/2/3^{S141} (Invitrogen), pCofilin^{S3} (Abcam), PAK3 (Millipore), or cofilin (Cytoskeleton, Inc.) and secondary antisera, including Alexa Fluor 488 anti–mouse and Alexa Fluor 594 anti–rabbit (Invitrogen; Chen et al., 2007).

Deconvolution microscopy and quantification of synaptic structures

Z-series (0.2-µm steps) images were acquired at 63× (Plan-Apochromat NA 1.4) using a microscope (DM6000; Leica) and a charge-coupled device camera (Orca ER; Hamamatsu Photonics). Images were collected from two to four sections situated 20–80 µm below the atmosphere interface of each slice. Iterative deconvolution (99% confidence) was performed by Volocity 4.1 (PerkinElmer). Point spread functions were calculated from multispectral microspheres (0.5-µm diameter; Invitrogen) in fixed tissue sections.

Labeled synaptic structures were measured and counted from a 136 × 105 × 3–µm (x, y, z) sampling zone in proximal str. radiatum between the two stimulating electrodes. Sample objects (i.e., pCofilin$^+$ elements) were small relative to image size (5.8 ± 0.3% cumulative object pixel area for PSD95$^+$ elements; n = 15), regularly shaped, and diffusely scattered throughout the image, thus allowing for automatic image correction, intensity normalization, and object identification. Acquisition-based nonuniformities were corrected point by point using white (illumination only) and dark (shutter closed) background images. The slow shading component was obtained by low-pass filter and removed from image z stacks. Intensity normalization to a target background level (15% of maximum) was performed on image subsections (10 × 10 × 1 µm) to standardize object quantification across sections and batches of tissue (Rout et al., 2004). Image manipulations were performed using Matlab 7 (Mathworks).

Object identification was performed using a 3D variant of an established protocol (Lin et al., 2005; Chen et al., 2007). Pixel values (8 bit) were iteratively binarized using a fixed interval intensity threshold series (4% intervals from 15–75% of maximum) followed by erosion and dilation filtering. This protocol reliably detected boundaries of both faintly and densely labeled punctate structures. Object area (>0.04 and <1.2 µm^3) and eccentricity criteria were applied to eliminate artifact. Phosphoprotein$^+$ and PSD95$^+$ objects were considered to reside in the same synapse if any overlap between their respective boundaries was detected. The isolated TBS component (TBSΔ) was calculated from double-labeled object counts (O) from TBS and control (CON) slices as follows: $TBS\Delta = (O_{TBS} - \overline{O}_{CON}) / \overline{O}_{CON}$. Image acquisition and analysis were conducted blind to treatment.

Western blot analysis

Samples (two to three pooled slices) were homogenized in radioimmunoprecipitation assay buffer containing 10 mM Tris, pH 7.2, 158 mM NaCl, 1 mM EDTA, 0.1% SDS, 1% Na-deoxycholate, 1% Triton X-100, 1× complete protease inhibitor cocktail (Roche), and phosphatase inhibitor cocktails 1–2 (Sigma-Aldrich; Rex et al., 2007). Samples were normalized by Bio-Rad protein assay and processed for Western blot analysis (12%

SDS-PAGE) using rabbit antisera to pCofilin^{S3}, pPAK1/2/3^{S141} (see Immunocytochemistry), or pPAK1/2/3^{T423} (Cell Signaling Technology) and the ECL Plus detection system (GE Healthcare). Blots were reblotted (Millipore) and probed for β-tubulin and β-actin (Sigma-Aldrich). Immunoreactive bands were measured using ImageJ (National Institutes of Health). *n* values represent the numbers of samples tested.

Pull-down assays for activated Rho GTPases

Samples (6–10 pooled slices) were homogenized in Mg^{2+} lysis buffer (Millipore) with complete protease inhibitor cocktail, normalized, and then assayed using RhoA or Cdc42/Rac pull-down kits (Millipore). Samples were incubated with Rac/Cdc42 (PAK1 PAK-binding domain) or RhoA (Rhotekin-binding domain) and rocked for 2 h. Rhotekin binds strongly to RhoA and RhoC (absent in brain) but weakly to RhoB (Reid et al., 1996); thus, only RhoA is detected with antisera to RhoA. Agarose beads were collected by centrifugation (for 10 s at 14,000 *g* and 4°C), washed, resuspended in Laemmli buffer, and boiled for 5 min. Western blot analysis (12% SDS-PAGE) used mouse anti-RhoA (Santa Cruz Biotechnology, Inc.), mouse anti-Rac (Millipore), or rabbit anti-Cdc42 (Millipore). GTP and GDP loading controls were incubated with 100 µM GTP-γS or 1 mM GDP for 30 min at 30°C.

Statistics

All values in figures, figure captions, and text represent group means ± SEM. Unless stated otherwise, group differences for single pulse stimulation (final 10 min of recording), input/output, PPF, and continuous PPF were assessed by repeated measures analysis of variance. For quantification of immunopositive elements and Western blots, statistical significance ($P \leq 0.05$) was determined by analysis of variance followed by Tukey's post hoc test or two-tailed Student's *t* test using SPSS 15.0 (SSPS, Inc.). Curve fitting and statistical tests were performed using Matlab 7.

Online supplemental material

Fig. S1 shows the effect of short adenosine infusions on LTP and presynaptic release probability when applied 2 or 10 min after TBS. Fig. S2 shows that JPK does not alter presynaptic release probability or acute responses to TBS. Fig. S3 describes the effects of chemically induced synaptic potentiation on Rho GTPases and PAK and cofilin activity. Fig. S4 shows that the ROCK inhibitor H1152 does not alter basic synaptic physiology or acute responses to potentiating stimuli. Fig. S5 shows the effects of the Rac inhibitor NSC23766 on spine F-actin in slices challenged with Lat A at 10 min after TBS. Video 1 shows representative labeling (3D reconstruction) for F-actin by phalloidin applied in situ from slices receiving TBS or control stimulation. Video 2 shows an example field (CA1 str. radiatum) reconstructed in three dimensions from pCofilin and PSD95 ir. Online supplemental material is available at http://www.jcb.org/cgi/content/full/jcb.200901084/DC1.

We thank Yas Sanaiha and Abhishek Chadha for technical support.

This research was supported by grants NS45260 and NS37799 from the National Institute of Neurological Disorders and Stroke (NINDS). C.S. Rex was supported by NINDS grant NS045540. L.Y. Chen was supported by National Institute of Mental Health grant MH083396.

Submitted: 19 January 2009
Accepted: 10 June 2009

References

Abraham, W.C. 2003. How long will long-term potentiation last? *Philos. Trans. R. Soc. Lond. B Biol. Sci.* 358:735–744.

Arai, A., J. Larson, and G. Lynch. 1990. Anoxia reveals a vulnerable period in the development of long-term potentiation. *Brain Res.* 511:353–357.

Boda, B., S. Alberi, I. Nikonenko, R. Node-Langlois, P. Jourdain, M. Moosmayer, L. Parisi-Jourdain, and D. Muller. 2004. The mental retardation protein PAK3 contributes to synapse formation and plasticity in hippocampus. *J. Neurosci.* 24:10816–10825.

Bokoch, G.M. 2003. Biology of the p21-activated kinases. *Annu. Rev. Biochem.* 72:743–781.

Carlisle, H.J., P. Manzerra, E. Marcora, and M.B. Kennedy. 2008. SynGAP regulates steady-state and activity-dependent phosphorylation of cofilin. *J. Neurosci.* 28:13673–13683.

Chen, L.Y., C.S. Rex, M.S. Casale, C.M. Gall, and G. Lynch. 2007. Changes in synaptic morphology accompany actin signaling during LTP. *J. Neurosci.* 27:5363–5372.

Chong, C., L. Tan, L. Lim, and E. Manser. 2001. The mechanism of PAK activation. Autophosphorylation events in both regulatory and kinase domains control activity. *J. Biol. Chem.* 276:17347–17353.

Cooper, J.A., and D. Sept. 2008. New insights into mechanism and regulation of actin capping protein. *Int. Rev. Cell Mol. Biol.* 267:183–206.

Deacon, S.W., A. Beeser, J.A. Fukui, U.E. Rennefahrt, C. Myers, J. Chernoff, and J.R. Peterson. 2008. An isoform-selective, small-molecule inhibitor targets the autoregulatory mechanism of p21-activated kinase. *Chem. Biol.* 15:322–331.

Fukazawa, Y., Y. Saitoh, F. Ozawa, Y. Ohta, K. Mizuno, and K. Inokuchi. 2003. Hippocampal LTP is accompanied by enhanced F-actin content within the dendritic spine that is essential for late LTP maintenance in vivo. *Neuron*. 38:447–460.

Gao, Y., J.B. Dickerson, F. Guo, J. Zheng, and Y. Zheng. 2004. Rational design and characterization of a Rac GTPase-specific small molecule inhibitor. *Proc. Natl. Acad. Sci. USA*. 101:7618–7623.

Gehler, S., G. Gallo, E. Veien, and P.C. Letourneau. 2004. p75 neurotrophin receptor signaling regulates growth cone filopodial dynamics through modulating RhoA activity. *J. Neurosci.* 24:4363–4372.

Gungabissoon, R.A., and J.R. Bamburg. 2003. Regulation of growth cone actin dynamics by ADF/cofilin. *J. Histochem. Cytochem.* 51:411–420.

Hayashi, M.L., S.Y. Choi, B.S. Rao, H.Y. Jung, H.K. Lee, D. Zhang, S. Chattarji, A. Kirkwood, and S. Tonegawa. 2004. Altered cortical synaptic morphology and impaired memory consolidation in forebrain- specific dominant-negative PAK transgenic mice. *Neuron*. 42:773–787.

Hayashi, M.L., B.S. Rao, J.S. Seo, H.S. Choi, B.M. Dolan, S.Y. Choi, S. Chattarji, and S. Tonegawa. 2007. Inhibition of p21-activated kinase rescues symptoms of fragile X syndrome in mice. *Proc. Natl. Acad. Sci. USA*. 104:11489–11494.

Huang, F., J.K. Chotiner, and O. Steward. 2007. Actin polymerization and ERK phosphorylation are required for Arc/Arg3.1 mRNA targeting to activated synaptic sites on dendrites. *J. Neurosci.* 27:9054–9067.

Huber, A.B., A.L. Kolodkin, D.D. Ginty, and J.F. Cloutier. 2003. Signaling at the growth cone: ligand-receptor complexes and the control of axon growth and guidance. *Annu. Rev. Neurosci.* 26:509–563.

Ireland, D.R., and W.C. Abraham. 2009. Mechanisms of group I mGluR-dependent long-term depression of NMDA receptor-mediated transmission at Schaffer collateral-CA1 synapses. *J. Neurophysiol.* 101:1375–1385.

Kim, C.H., and J.E. Lisman. 1999. A role of actin filament in synaptic transmission and long-term potentiation. *J. Neurosci.* 19:4314–4324.

Kramar, E.A., B. Lin, C.S. Rex, C.M. Gall, and G. Lynch. 2006. Integrin-driven actin polymerization consolidates long-term potentiation. *Proc. Natl. Acad. Sci. USA*. 103:5579–5584.

Krucker, T., G.R. Siggins, and S. Halpain. 2000. Dynamic actin filaments are required for stable long-term potentiation (LTP) in area CA1 of the hippocampus. *Proc. Natl. Acad. Sci. USA*. 97:6856–6861.

Kuhn, T.B., P.J. Meberg, M.D. Brown, B.W. Bernstein, L.S. Minamide, J.R. Jensen, K. Okada, E.A. Soda, and J.R. Bamburg. 2000. Regulating actin dynamics in neuronal growth cones by ADF/cofilin and rho family GTPases. *J. Neurobiol.* 44:126–144.

Larson, J., P. Xiao, and G. Lynch. 1993. Reversal of LTP by theta frequency stimulation. *Brain Res.* 600:97–102.

Lin, B., E.A. Kramar, X. Bi, F.A. Brucher, C.M. Gall, and G. Lynch. 2005. Theta stimulation polymerizes actin in dendritic spines of hippocampus. *J. Neurosci.* 25:2062–2069.

Linseman, D.A., and F.A. Loucks. 2008. Diverse roles of Rho family GTPases in neuronal development, survival, and death. *Front. Biosci.* 13:657–676.

Lynch, G., and M. Baudry. 1984. The biochemistry of memory: a new and specific hypothesis. *Science*. 224:1057–1063.

Lynch, G., C.S. Rex, and C.M. Gall. 2007. LTP consolidation: substrates, explanatory power, and functional significance. *Neuropharmacology*. 52:12–23.

Matus, A., M. Ackermann, G. Pehling, H.R. Byers, and K. Fujiwara. 1982. High actin concentrations in brain dendritic spines and postsynaptic densities. *Proc. Natl. Acad. Sci. USA*. 79:7590–7594.

Meng, J., Y. Meng, A. Hanna, C. Janus, and Z. Jia. 2005. Abnormal long-lasting synaptic plasticity and cognition in mice lacking the mental retardation gene Pak3. *J. Neurosci.* 25:6641–6650.

Messaoudi, E., T. Kanhema, J. Soule, A. Tiron, G. Dagyte, B. da Silva, and C.R. Bramham. 2007. Sustained Arc/Arg3.1 synthesis controls long-term potentiation consolidation through regulation of local actin polymerization in the dentate gyrus in vivo. *J. Neurosci.* 27:10445–10455.

Morris, R.G., E.I. Moser, G. Riedel, S.J. Martin, J. Sandin, M. Day, and C. O'Carroll. 2003. Elements of a neurobiological theory of the hippocampus: the role of activity-dependent synaptic plasticity in memory. *Philos. Trans. R. Soc. Lond. B Biol. Sci.* 358:773–786.

Niwa, R., K. Nagata-Ohashi, M. Takeichi, K. Mizuno, and T. Uemura. 2002. Control of actin reorganization by Slingshot, a family of phosphatases that dephosphorylate ADF/cofilin. *Cell*. 108:233–246.

O'Kane, E.M., T.W. Stone, and B.J. Morris. 2004. Increased long-term potentiation in the CA1 region of rat hippocampus via modulation of GTPase signalling or inhibition of Rho kinase. *Neuropharmacology*. 46:879–887.

Racz, B., and R.J. Weinberg. 2006. Spatial organization of cofilin in dendritic spines. *Neuroscience*. 138:447–456.

Reid, T., T. Furuyashiki, T. Ishizaki, G. Watanabe, N. Watanabe, K. Fujisawa, N. Morii, P. Madaule, and S. Narumiya. 1996. Rhotekin, a new putative target for Rho bearing homology to a serine/threonine kinase, PKN, and rhophilin in the Rho-binding domain. *J. Biol. Chem.* 271:13556–13560.

Rex, C.S., C.Y. Lin, E.A. Kramar, L.Y. Chen, C.M. Gall, and G. Lynch. 2007. Brain-derived neurotrophic factor promotes long-term potentiation-related cytoskeletal changes in adult hippocampus. *J. Neurosci.* 27:3017–3029.

Rosso, L., P.M. Pierson, C. Golfier, B. Peteri-Brunback, C. Deroanne, E. Van Obberghen-Schilling, and J.M. Mienville. 2007. Pituicyte stellation is prevented by RhoA-or Cdc42-dependent actin polymerization. *Cell. Mol. Neurobiol.* 27:791–804.

Roth-Alpermann, C., R.G. Morris, M. Korte, and T. Bonhoeffer. 2006. Homeostatic shutdown of long-term potentiation in the adult hippocampus. *Proc. Natl. Acad. Sci. USA*. 103:11039–11044.

Rout, S., V. Lam, A.E. Bell, and K.A. Duca. 2004. Epi-fluorescent image modeling for viral infection analysis. *Conference Record of the Thirty-Eighth Asilomar Conference on Signals, Systems and Computers*. 2:1841–1846.

Sacktor, T.C. 2008. PKMzeta, LTP maintenance, and the dynamic molecular biology of memory storage. *Prog. Brain Res.* 169:27–40.

Sasaki, Y., M. Suzuki, and H. Hidaka. 2002. The novel and specific Rho-kinase inhibitor (S)-(+)-2-methyl-1-[(4-methyl-5-isoquinoline)sulfonyl]-homopiperazine as a probing molecule for Rho-kinase-involved pathway. *Pharmacol. Ther.* 93:225–232.

Semenova, M.M., A.M. Maki-Hokkonen, J. Cao, V. Komarovski, K.M. Forsberg, M. Koistinaho, E.T. Coffey, and M.J. Courtney. 2007. Rho mediates calcium-dependent activation of p38alpha and subsequent excitotoxic cell death. *Nat. Neurosci.* 10:436–443.

Smart, F.M., G.M. Edelman, and P.W. Vanderklish. 2003. BDNF induces translocation of initiation factor 4E to mRNA granules: evidence for a role of synaptic microfilaments and integrins. *Proc. Natl. Acad. Sci. USA*. 100:14403–14408.

Soderling, S.H., E.S. Guire, S. Kaech, J. White, F. Zhang, K. Schutz, L.K. Langeberg, G. Banker, J. Raber, and J.D. Scott. 2007. A WAVE-1 and WRP signaling complex regulates spine density, synaptic plasticity, and memory. *J. Neurosci.* 27:355–365.

Takahashi, K., and K. Suzuki. 2009. Membrane transport of WAVE2 and lamellipodia formation require Pak1 that mediates phosphorylation and recruitment of stathmin/Op18 to Pak1-WAVE2-kinesin complex. *Cell. Signal.* 21:695–703.

Tashiro, A., A. Minden, and R. Yuste. 2000. Regulation of dendritic spine morphology by the rho family of small GTPases: antagonistic roles of Rac and Rho. *Cereb. Cortex*. 10:927–938.

Thaxton, C., J. Lopera, M. Bott, M.E. Baldwin, P. Kalidas, and C. Fernandez-Valle. 2007. Phosphorylation of the NF2 tumor suppressor in Schwann cells is mediated by Cdc42-Pak and requires paxillin binding. *Mol. Cell. Neurosci.* 34:231–242.

Thirone, A.C., P. Speight, M. Zulys, O.D. Rotstein, K. Szászi, S.F. Pedersen, and A. Kapus. 2009. Hyperosmotic stress induces Rho/Rho kinase/LIM kinase-mediated cofilin phosphorylation in tubular cells: key role in the osmotically triggered F-actin response. *Am. J. Physiol. Cell Physiol.* 296:C463–C475.

van Galen, E.J., and G.J. Ramakers. 2005. Rho proteins, mental retardation and the neurobiological basis of intelligence. *Prog. Brain Res.* 147:295–317.

Wall, M.J., and N. Dale. 2007. Auto-inhibition of rat parallel fibre-Purkinje cell synapses by activity-dependent adenosine release. *J. Physiol.* 581:553–565.

Wang, H.G., F.M. Lu, I. Jin, H. Udo, E.R. Kandel, J. de Vente, U. Walter, S.M. Lohmann, R.D. Hawkins, and I. Antonova. 2005. Presynaptic and postsynaptic roles of NO, cGK, and RhoA in long-lasting potentiation and aggregation of synaptic proteins. *Neuron*. 45:389–403.

Webb, B.A., S. Zhou, R. Eves, L. Shen, L. Jia, and A.S. Mak. 2006. Phosphorylation of cortactin by p21-activated kinase. *Arch. Biochem. Biophys.* 456:183–193.

Zhou, Q., M. Xiao, and R.A. Nicoll. 2001. Contribution of cytoskeleton to the internalization of AMPA receptors. *Proc. Natl. Acad. Sci. USA*. 98:1261–1266.